




## Article

# Vector Beams with Only Transverse Intensity at Focus

Sergey S. Stafeev <sup>1,2</sup>, Nikita N. Kazakov <sup>2</sup>, Vladislav D. Zaitsev <sup>1,2,\*</sup>, Sergey D. Poletayev <sup>1</sup>  
and Victor V. Kotlyar <sup>1,2</sup>

<sup>1</sup> Laser Measurements Laboratory, IPSI RAS—Branch of the FSRC “Crystallography and Photonics” RAS, Molodogvardeyskaya 151, 443001 Samara, Russia; sergey.stafeev@gmail.com (S.S.S.); sergpolet@gmail.com (S.D.P.); kotlyar@ipsiras.ru (V.V.K.)

<sup>2</sup> Technical Cybernetics Department, Samara National Research University, Moskovskoye Shosse 34, 443086 Samara, Russia; nikita37pobeditel@mail.ru

\* Correspondence: zaicev-vlad@yandex.ru

**Abstract:** In this work, the tight focusing of vector beams with azimuthal polarization and beams with a V-line of polarization singularity (sector azimuthal polarization) was simulated numerically using the Richards–Wolf formulas. It was demonstrated that in a tight focus for these beams, there is no longitudinal component of the electric field. Previously, a similar effect was demonstrated for azimuthally polarized light only. The longitudinal component of the spin angular momentum for these beams was calculated, and the possibility of creating sector azimuthally polarized beams (beams with V-line singularities) using vector waveplates was demonstrated.

**Keywords:** tight focusing; vector beam; azimuthal polarization; spin angular momentum; magnetization

## 1. Introduction

Currently, there is a growing interest of researchers in the use of azimuthally polarized light [1]. Initially, azimuthal polarization was proposed to obtain compact spots [2,3]. However, later other applications were demonstrated. For example, in [4,5], an azimuthally polarized beam was used to generate the third harmonic in ensembles of silicon nanoparticles (quadrumers and trimers). It is azimuthally polarized light that turned out to be the most suitable for the excitation of Mie resonances in the oligomers under study: generation was improved by two orders of magnitude compared to using linear polarization. In [6], a fiber-optic sensor was proposed in which the azimuthally polarized mode propagated as the fundamental mode.

Quite intriguing is the use of azimuthally polarized light for manipulation of magnetization, which is calculated as the vector product of the electric field and its complex conjugation:  $\mathbf{M} \sim \mathbf{E} \times \mathbf{E}^*$ . The increased interest in the study of magnetization is caused by their possible application in optomagnetic memory systems [7,8]. Due to the absence of a longitudinal component of the electric field, the magnetization in an azimuthally polarized vortex beam is always directed along the propagation axis. In this way, it has been possible to obtain spots [9], needles [10–12], chains [13–15], and arrays of magnetization [16]. In [17], an increase in the magnetic field was observed at the center of quadrupoles and hexapoles made of silicon microspheres when they were illuminated by light with azimuthal polarization.

It should be noted that in a classical azimuthally polarized beam, the polarization direction changes continuously [1]. In this paper, we will show that similar properties to azimuthally polarized beams can also be obtained for sectoral azimuthally polarized beams containing V-lines of singularity. Previously, similar piecewise continuous polarization states were investigated in [18–20]. In [18], optical vortices with cylindrical polarization of half-integer orders were studied. In [19], the focusing of cylindrical vector beams of fractional orders was numerically simulated, and in [20], a vector beam that was formed from



**Citation:** Stafeev, S.S.; Kazakov, N.N.; Zaitsev, V.D.; Poletayev, S.D.; Kotlyar, V.V. Vector Beams with Only Transverse Intensity at Focus. *Appl. Sci.* **2023**, *13*, 12519. <https://doi.org/10.3390/app132212519>

Academic Editor: Jesús Liñares Beiras

Received: 30 September 2023

Revised: 9 November 2023

Accepted: 17 November 2023

Published: 20 November 2023



**Copyright:** © 2023 by the authors. Licensee MDPI, Basel, Switzerland. This article is an open access article distributed under the terms and conditions of the Creative Commons Attribution (CC BY) license (<https://creativecommons.org/licenses/by/4.0/>).

two other vector beams was considered—the upper part of the beam had one order, and the lower half had another order. Initially, there was no longitudinal spin angular momentum in these beams [19,20]: the polarization at each point of the initial beam was linear; however, with tight focusing, a nonzero longitudinal component of the spin angular momentum arose, which indicated the appearance of regions in which the polarization is elliptical. This effect is a special case of spin–orbit interaction in a tight focus. Beams with discontinuities in polarization can be created using metasurfaces based on superoscillations [21] or subwavelength gratings [22].

In this work, tight focusing of vector beams with azimuthal polarization and beams with V-lines of polarization singularity was simulated numerically using the Richards–Wolf formula. It was demonstrated that in a tight focus for these beams, there is no longitudinal component of the electric field. Previously, a similar effect was demonstrated for azimuthally polarized beams only. The absence of a longitudinal component of the electric field leads to the absence of transverse components of the spin angular momentum and transverse components of magnetization. This characteristic of the investigated beams can be used to obtain pure longitudinal magnetization distributions, for example in optomagnetic memory systems [7,8]. The possibility of creating sectorial azimuthally polarized beams using vector wave plates and spatial light modulators was experimentally demonstrated. The intensity distribution patterns measured in the experiment were consistent with the simulation results.

## 2. Methods

### 2.1. Numerical Simulation

The simulation in this work was carried out by the calculation of the Richards–Wolf integral [23,24], in which the electric field at the focus of a high numerical aperture lens is calculated by the equation:

$$\mathbf{E}(\rho, \psi, z) = -\frac{if}{\lambda} \int_0^\alpha \int_0^{2\pi} B(\theta, \varphi) T(\theta) \mathbf{P}(\theta, \varphi) \times \exp\{ik[\rho \sin \theta \cos(\varphi - \psi) + z \cos \theta]\} \sin \theta \, d\theta \, d\varphi, \tag{1}$$

where  $B(\theta, \varphi)$  is the electric field of the incident beam (before the focusing lens);  $\theta$  and  $\varphi$  are the polar and the azimuthal angles;  $T(\theta)$  is the apodization function, which characterizes the focusing lens (for example, it is equal to  $T(\theta) = \cos(\theta)^{1/2}$  for aplanatic lenses [24], or  $T(\theta) = \cos(\theta)^{-3/2}$  for zone plates [25]);  $f$  is the focal length;  $k = 2\pi/\lambda$  is the wavenumber;  $\lambda$  is the wavelength;  $\alpha$  is the maximum polar angle, which is defined by the numerical aperture of the lens  $\alpha = \arcsin(\text{NA})$ ; and  $\mathbf{P}(\theta, \varphi)$  is the polarization vector:

$$\mathbf{P}(\theta, \varphi) = \begin{bmatrix} 1 + \cos^2 \varphi (\cos \theta - 1) \\ \sin \varphi \cos \varphi (\cos \theta - 1) \\ -\sin \theta \cos \varphi \end{bmatrix} a(\theta, \varphi) + \begin{bmatrix} \sin \varphi \cos \varphi (\cos \theta - 1) \\ 1 + \sin^2 \varphi (\cos \theta - 1) \\ -\sin \theta \sin \varphi \end{bmatrix} b(\theta, \varphi), \tag{2}$$

where  $a(\theta, \varphi)$  and  $b(\theta, \varphi)$  are functions describing the state of polarization of the  $x$ - and  $y$ -components of the incident beam. The Richards–Wolf integral (1) is used to calculate the components of the electric and magnetic fields at the focus of a high numerical aperture lens because it allows calculation in a vector approximation—it calculates not only the transverse field components but also the longitudinal component. The Richards–Wolf integral is valid if the focal length is much longer than the wavelength of the focused light. For simplicity of calculations, it was assumed in the simulation that the zone plate ( $T(\theta) = \cos(\theta)^{-3/2}$  [25]) with  $\text{NA} = 0.95$  focusing the plane wave  $B(\theta, \varphi) = 1$  in air  $n = 1$ .

In this work, vector beams with sector azimuthal polarization are investigated. Figure 1 shows the direction of polarization of the studied beams: Figure 1a shows the direction for

an azimuthally polarized beam; Figure 1b,c show the direction of polarization of a beam with a V-line singularity [26]; Figure 1d shows the polarization of a beam with two V-line singularities. It should be noted that the direction of polarization of the beam in Figure 1b coincides with the direction of polarization of an azimuthally polarized beam that has passed through a binary step [27,28].

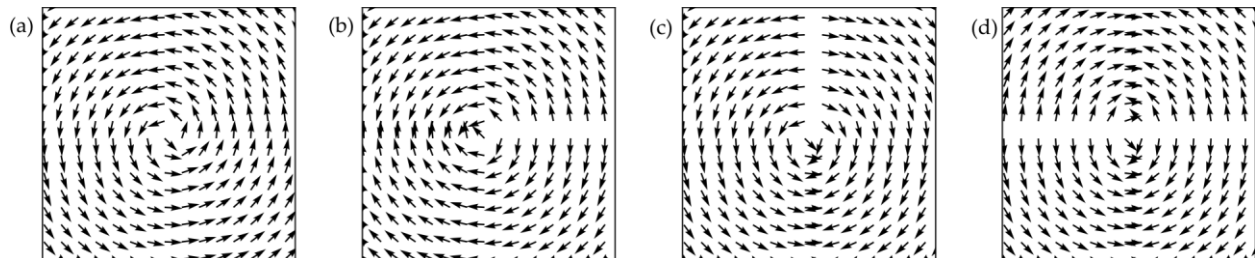


**Figure 1.** Direction of polarization of the investigated vector beams: azimuthally polarized (a), and sector azimuthally polarized: beams with a V-line singularity (b,c), and beam with two V-line singularities (d).

## 2.2. Experimental Measurement

To obtain vector beams with polarization shown in Figure 1a, a vector wave plate could be used; however, to obtain the polarization state shown in Figure 1b,c, this vector wave plate should be combined with a spatial light modulator. In our experimental measurements (Figure 2), laser light from MGL-F-532-700 (wavelength  $\lambda = 532$  nm, output power 700 mW) was collimated by a pinhole PH (diameter  $D = 50$   $\mu\text{m}$ ) and a spherical lens ( $L_1$ ) ( $f_1 = 400$  mm). After the lens  $L_1$ , the expanded beam propagates through the transmissive spatial light modulator (SLM, Holoeye LC2012, resolution of  $1024 \times 768$  pixels, pixel size of 36  $\mu\text{m}$ , Tokyo, Japan). SLM was placed between two linear polarizers  $P_1$  and  $P_2$  to obtain a linearly polarized beam after phase modulation. Lenses  $L_2$  and  $L_3$  and iris diaphragm D were used to spatially filter the desired beam. Then, the beam was aligned with the center of the vector wave plate (VWP, LBTEK VR1, Shenzhen, China). The resulting beam was focused by a lens with a small numerical aperture  $L_4$  ( $f_4 = 100$  mm). Objective lens  $O_1$  (Olympus RMS 20X, Tokyo, Japan) was used to obtain an image at the focus of the lens  $L_4$ , and the image was projected onto a CCD camera (UCMOS10000KPA, resolution of  $3584 \times 2748$  pixels, pixel size of 1.67  $\mu\text{m}$ , Hangzhou, China), in front of which a linear polarizer-analyzer  $P_3$  was placed.

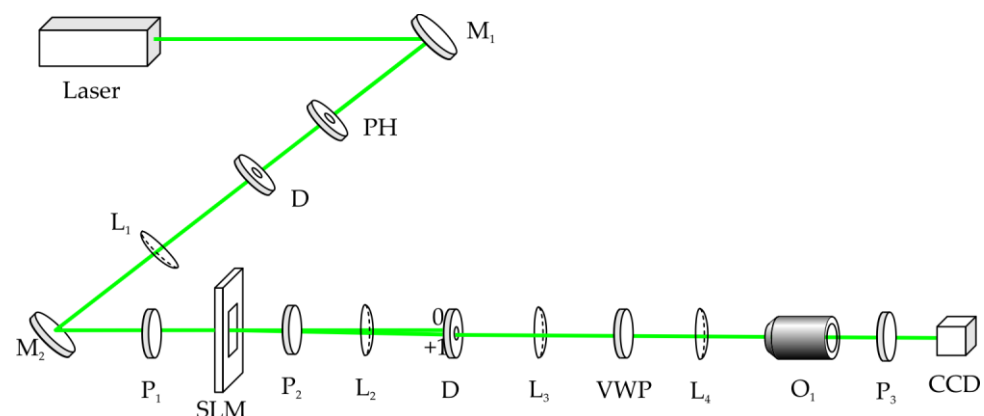


**Figure 2.** Laser—MGL-F-532-700 ( $\lambda = 532$  nm);  $M_1$ ,  $M_2$ —mirrors; PH—pinhole (diameter of 50  $\mu\text{m}$ );  $L_1$ – $L_4$ —lenses ( $f_1 = 400$  mm,  $f_2 = 150$  mm,  $f_3 = 125$  mm,  $f_4 = 100$  mm);  $O_1$ —objective lens (Olympus RMS 20X); D—iris diaphragm; SLM—spatial light modulator (Holoeye LC 2012, resolution of  $1024 \times 768$  pixels, pixel size of 36  $\mu\text{m}$ );  $P_1$ – $P_3$ —linear polarizers; VWP—vector wave plate (LBTEK VR1); CCD—CCD camera (UCMOS10000KPA, resolution of  $3584 \times 2748$  pixels, pixel size of 1.67  $\mu\text{m}$ ).

### 3. Results

#### 3.1. Azimuthally Polarized Light

The polarization at which the electric field is directed strictly azimuthally is well known. The absence of the longitudinal component of the electric field, in this case, follows directly from Maxwell’s vector equations written for a cylindrical coordinate system: when the derivative with respect to the azimuthal angle is set to zero, the system of six equations is divided into two systems of equations, each containing three equations (an analogy can be seen with TE- and TM-polarization in a Cartesian coordinate system). One of the systems is:

$$\begin{cases} \frac{\partial H_\rho}{\partial z} - \frac{\partial H_z}{\partial \rho} = \epsilon \epsilon_0 \frac{\partial E_\varphi}{\partial t} + \sigma E_\varphi, \\ -\frac{\partial E_\varphi}{\partial z} = -\mu \mu_0 \frac{\partial H_\rho}{\partial t}, \\ \frac{1}{\rho} \frac{\partial(\rho E_\varphi)}{\partial \rho} = -\mu \mu_0 \frac{\partial H_z}{\partial t}, \end{cases} \quad (3)$$

where  $\mathbf{H}$  is the magnetic field,  $\epsilon$  and  $\mu$  are the dielectric and magnetic permeability, and  $\epsilon_0$  and  $\mu_0$  are the electric and magnetic constants. The field described by (3) contains only one electrical field component  $E_\varphi$ .

For a classical azimuthally polarized beam, the electric field component of the initial beam in (1) has the form:

$$E(\theta, \varphi) = \begin{pmatrix} a(\varphi) \\ b(\varphi) \end{pmatrix} = \begin{pmatrix} -\sin \varphi \\ \cos \varphi \end{pmatrix}. \quad (4)$$

Substituting Equation (4) into (2), we can see that

$$P_z(\theta, \varphi) = \sin \theta \cos \varphi \sin \varphi - \sin \theta \sin \varphi \cos \varphi = 0. \quad (5)$$

Previously, only the case of azimuthal polarization was studied (without singularity lines). Azimuthal polarization is a special case of a beam with a V-point singularity [26] located at the center of the beam.

The result of focusing an azimuthally polarized beam (4), calculated by (1), is shown in Figure 3. The distribution of intensity  $I = |E_x|^2 + |E_y|^2 + |E_z|^2$  (Figure 3a) and its individual components are shown. From Figure 3d, it can be seen that the longitudinal component is equal to zero.

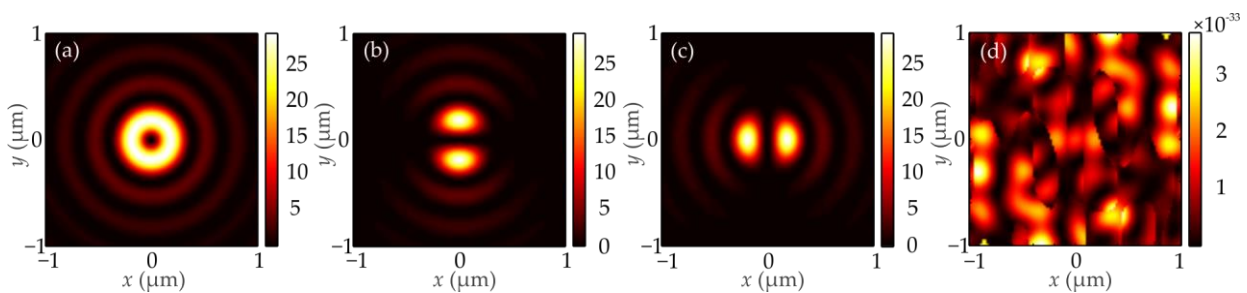


**Figure 3.** Intensity  $I$  (a) and its individual components  $I_x$  (b),  $I_y$  (c), and  $I_z$  (d) at the focus of a beam with azimuthal polarization (4).

It should be noted that the absence of the longitudinal component of the electric field leads to the fact that the spin angular momentum (SAM) vector will contain the longitudinal component only (or  $S_z \equiv 0$ ):

$$\mathbf{S} = \frac{1}{8\pi\omega} \text{Im}(\mathbf{E}^* \times \mathbf{E}), \quad (6)$$

where  $\omega$  is the angular frequency of the light (the constant  $1/(8\pi\omega)$  will be then omitted), sign “\*” means complex conjugation. It should be noted that the spin angular momentum

(6) is opposite, and differs in absolute value only by a factor from the magnetization vector:

$$\mathbf{M} = i\gamma[\mathbf{E} \times \mathbf{E}^*], \tag{7}$$

where  $\gamma$  is the magneto-optical susceptibility.

Previously [29], it was shown that the components of the electric field for azimuthally polarized light have the form:

$$\begin{aligned} E_x &= -\sin \varphi [I_1 - I_2], \\ E_y &= \cos \varphi [I_1 - I_2], \\ E_z &= 0, \end{aligned} \tag{8}$$

where

$$\begin{aligned} I_1 &= \frac{\pi f}{\lambda} \int_0^\alpha T(\theta) \sin \theta (1 + \cos \theta) B(\theta) e^{ikz \cos \theta} J_1(x) d\theta, \\ I_2 &= \frac{\pi f}{\lambda} \int_0^\alpha T(\theta) \sin \theta (1 - \cos \theta) B(\theta) e^{ikz \cos \theta} J_{-1}(x) d\theta. \end{aligned} \tag{9}$$

In (9),  $x = krsin\theta$ ,  $J_m(x)$  is the  $m$ th order Bessel function, and  $B(\theta)$  is a real function describing the input field amplitude in the plane of the entrance pupil of the aplanatic system, depending only on the angle  $\theta$ . By substituting (8) into (6), we can show that the longitudinal component of the SAM in focus is equal to zero.

To obtain azimuthally polarized light, there are currently commercially available vector wave plates (we used LBTEK VR1). Linearly polarized light incident on such an element along the  $x$ -axis is converted into an azimuthally polarized beam, and linearly polarized along the  $y$ -axis into a radially polarized beam, thus creating the Jones matrix:

$$J_{CVB-1} = \begin{pmatrix} -\sin \varphi & \cos \varphi \\ \cos \varphi & \sin \varphi \end{pmatrix}. \tag{10}$$

Figure 4 shows an image of a beam obtained by propagating linearly polarized light (from laser MGL-F-532-700 with a wavelength  $\lambda$  of 532 nm and an output power of 700 mW) through a vector wave plate (VWP, LBTEK VR1) at different positions of the linear polarizer-analyzer P in front of the recording CCD camera (UCMOS10000KPA).

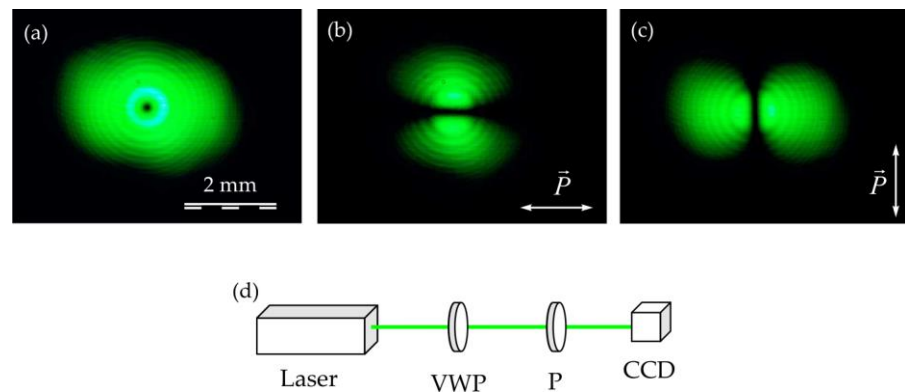


**Figure 4.** Image of an azimuthally polarized beam on a camera without an analyzer (a) and with an analyzer rotated by angle of  $0^\circ$  (b) and  $90^\circ$  (c). Experimental setup used to obtain the images (d): laser—MGL-F-532-700 ( $\lambda = 532$  nm, output power 700 mW); P—linear polarizer; VWP—vector wave plate (LBTEK VR1); CCD—CCD camera (UCMOS10000KPA).

Figure 4 shows that the beam polarization corresponds to the azimuthal one. The intensity distribution in Figure 4 corresponds to the distribution in Figure 3.

3.2. Beam with a V-Line of Polarization Singularity—Sector Azimuthal Polarization

It is possible to obtain other beams that do not have the z-component of the electric field. It is possible if, in addition to the V-point singularity, the beam contains V-line singularities [26]. The polarization functions of the initial field (1), in this case, are [30]:

$$E(\theta, \varphi) = \begin{pmatrix} a(\varphi) \\ b(\varphi) \end{pmatrix} = \begin{pmatrix} \cos(2\varphi) - 1 \\ \sin(2\varphi) \end{pmatrix}. \tag{11}$$

Substituting (11) into (2), we can show that:

$$P_z(\theta, \varphi) = -\sin \theta \cos \varphi (\cos(2\varphi) - 1) - \sin \theta \sin \varphi \sin(2\varphi) = -\sin \theta \left\{ -\cos \varphi + \underbrace{\cos \varphi \cos(2\varphi) + \sin \varphi \sin(2\varphi)}_{\cos \varphi} \right\} = 0. \tag{12}$$

Figure 5 shows the distribution of the intensity and its individual components in the focal plane for the beam (11). Figure 6 shows the distribution of the longitudinal component of the SAM at a distance  $\lambda$  from the focus: directly at the focus for this beam, all SAM components are equal to zero [30]. If a beam contains regions of nonzero longitudinal SAM, then the polarization in these regions is elliptical (or circular). Figure 6 shows that the plane contains four local regions of approximately 500 nm width, in which the light is circularly polarized along different diagonals. The initial beam has no points with circular polarization in its section (Figure 1). This conversion is a particular case of the Hall effect at a tight focus [30–33].

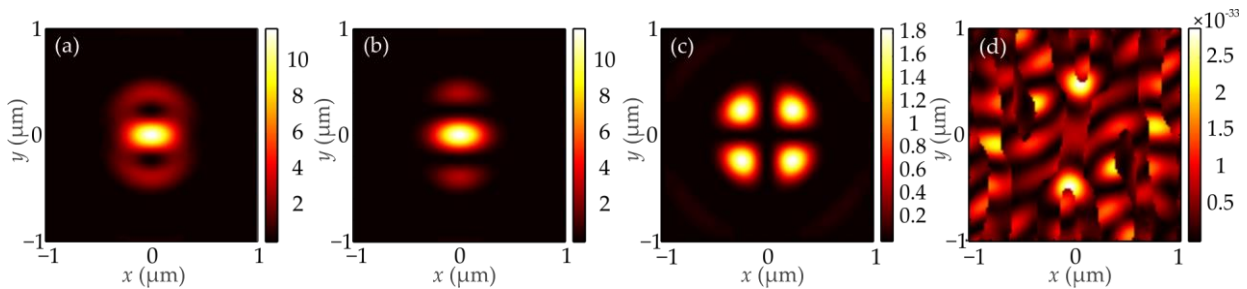


Figure 5. Intensity  $I$  (a) and its components  $I_x$  (b),  $I_y$  (c), and  $I_z$  (d) at the focus of the beam with the V-line of polarization singularity (11).

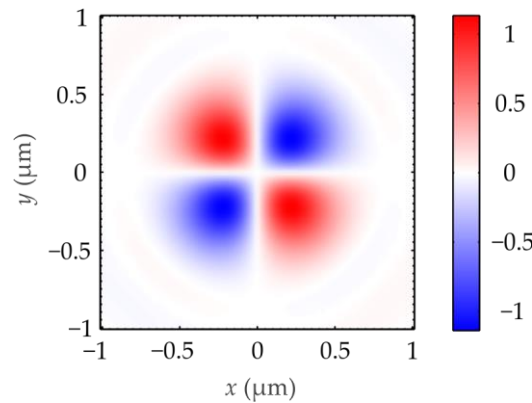


Figure 6. Distribution of the longitudinal component of the spin angular momentum  $SAM_z$  at a distance  $z = \lambda$  from the focus of the beam with the V-line of polarization singularity (11).



A similar beam with a rotated V-line of singularity has the form (Figure 1c):

$$\begin{aligned} a(\varphi) &= \sin(2\varphi), \\ b(\varphi) &= -\cos(2\varphi) - 1. \end{aligned} \tag{13}$$

This beam has the same distributions of intensity and longitudinal SAM, but rotated by 90 degrees.

Beam (11) (Figure 1b) can be experimentally obtained using the experimental setup shown on Figure 2. To do this, it is possible to pass a beam linearly polarized along the  $x$  axis through element (10); however, the polarization of the lower segment should differ in sign from the upper segment. Then, the polarization for the upper beam segment can be described by the Jones vector:

$$E = \begin{pmatrix} -\sin \varphi & \cos \varphi \\ \cos \varphi & \sin \varphi \end{pmatrix} \begin{pmatrix} 1 \\ 0 \end{pmatrix} = \begin{pmatrix} -\sin \varphi \\ \cos \varphi \end{pmatrix} \tag{14}$$

and for the bottom sector by the Jones vector:

$$E = \begin{pmatrix} -\sin \varphi & \cos \varphi \\ \cos \varphi & \sin \varphi \end{pmatrix} \begin{pmatrix} -1 \\ 0 \end{pmatrix} = \begin{pmatrix} \sin \varphi \\ -\cos \varphi \end{pmatrix} \tag{15}$$

To obtain polarization described by Equation (11) or Equations (14) and (15), a vertically divided screen was displayed on the SLM in such a way that a phase shift of  $\pi$  occurred in the lower part of the beam. The result of focusing is shown in Figure 7.

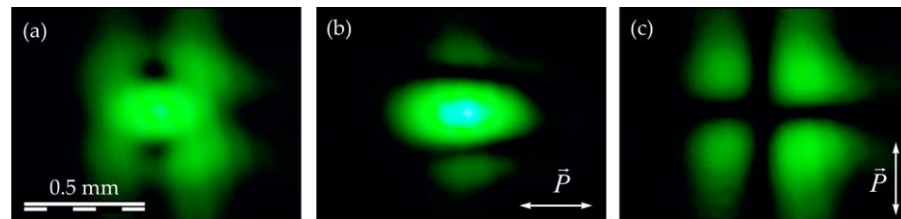


**Figure 7.** Image of a sector azimuthally polarized beam (11) on a camera without an analyzer (a) and with an analyzer rotated at an angle of 0° (b) and 90° (c).

Figure 7 shows that despite the small numerical aperture of the focusing lens, the intensity distribution pattern at the focus is consistent with the simulation (Figure 5). The slight asymmetry could be explained by the imperfection of the experiment. The beam center should be precisely positioned on both the SLM center (Figure 2) and the center of vector wave plate.

### 3.3. Beam with Two V-Lines of Polarization Singularity

It is also possible to shape the direction of polarization sector-by-sector. For example, the 1st and 3rd sectors have the polarization ( $a(\varphi) = -\sin(\varphi)$ ,  $b(\varphi) = \cos(\varphi)$ ), and the 2nd and 4th have the polarization ( $a(\varphi) = \sin(\varphi)$ ,  $b(\varphi) = -\cos(\varphi)$ ).

$$\begin{aligned} a(\varphi) &= \begin{cases} -\sin(\varphi), & 0 < \varphi \leq \pi/2, \quad \pi < \varphi \leq 3\pi/2 \\ \sin(\varphi), & \pi/2 < \varphi \leq \pi, \quad 3\pi/2 < \varphi \leq 2\pi \end{cases} \\ b(\varphi) &= \begin{cases} \cos(\varphi), & 0 < \varphi \leq \pi/2, \quad \pi < \varphi \leq 3\pi/2 \\ -\cos(\varphi), & \pi/2 < \varphi \leq \pi, \quad 3\pi/2 < \varphi \leq 2\pi \end{cases} \end{aligned} \tag{16}$$

Such a vector field will have two V-lines of polarization singularity (Figure 1d). For this case, the result of focusing is shown in Figures 8 and 9. Figure 8 shows the intensity and its components, and Figure 9 shows longitudinal component of the SAM in the focus plane ( $z = 0$ ).

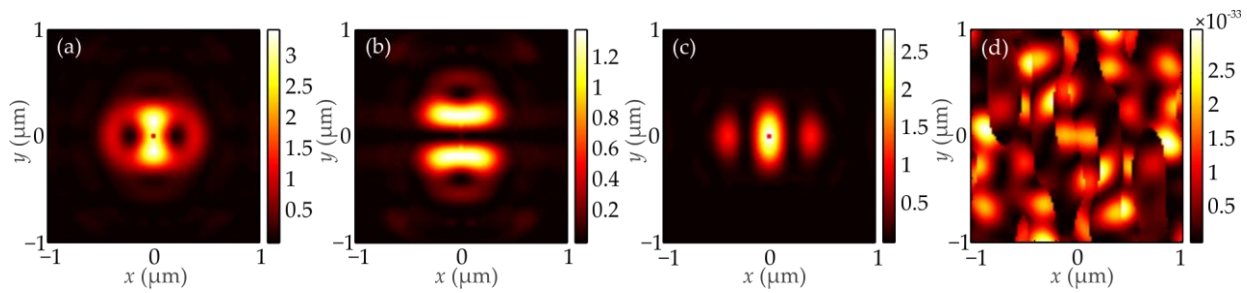


**Figure 8.** Intensity  $I$  (a) and its components  $I_x$  (b),  $I_y$  (c), and  $I_z$  (d) at the focus of the beam with two V-lines of polarization singularity.

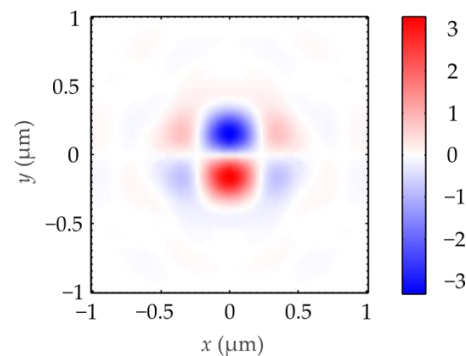


**Figure 9.** Distribution of the longitudinal component of the spin angular momentum  $SAM_z$  at the focus of the beam with two V-lines of polarization singularity.

Figure 9 also demonstrates the Hall effect at a tight focus.

#### 4. Discussion

In this paper, we investigated vector beams with azimuthal (Figure 1a) and sector azimuthal polarization (Figure 1b–d). Sector azimuthal polarization contains V-lines of polarization singularity. The absence of the longitudinal component of the electric field for these beams follows directly from the Maxwell Equation (3).

Tight focusing characteristics of the studied beams were investigated using the Richards–Wolf integral (1). The absence of the longitudinal component of the electric field was numerically proven (Figures 3d, 5d, and 8d). The intensity pattern of the transverse component differs for the investigated beams. Azimuthally polarized light (Figure 1a) has a doughnut-shaped structure (Figure 3a); however, the beams with V-line singularity (Figure 1b,d) have a peak-shaped focal spot (Figures 5a and 8a, consequently). In other words, all the studied beams do not have a longitudinal component of the electrical field; however, at the same time, they have different intensity shapes—peak or doughnut—and as a result, they could be used in different applications, where different shapes of transverse intensity without longitudinal intensity are needed.

Experimentally, the investigated beams with V-line polarization singularity (Figure 1b–d) could be generated using a vector wave plate and a spatial light modulator. The vector wave plate rotates the direction of polarization and converts the linearly polarized light to the beam with azimuthal polarization (Figure 1a). The example of an azimuthally polarized beam obtained after passing the linearly polarized beam through a vector wave plate is shown in Figure 4. Moreover, if the incident beam has sector linearly polarized light (for example, the Gauss–Hermite beam (0.1)), then after passing the vector wave plate, the output beam has sector azimuthal polarization. A beam with sector linear polarization could be generated using a spatial light modulator. Therefore, a spatial light modulator combined with a vector wave plate could be used to obtain the investigated sector azimuthal beams (Figure 2). The example of the focused beam with V-line singularity is shown in Figure 7. The intensity distribution pattern at the focus was consistent with the simulation.



It should be noted that due to the absence of the longitudinal component of the electric field  $E_z$ , the investigated beams do not contain transverse components of spin angular momentum ( $S_x = S_y = 0$ ). It is equivalent to the absence of transverse components of magnetization because the magnetization contains the same non-zero components as SAM. Moreover, the longitudinal component of SAM of the pure azimuthally polarized beam (Equation (4), Figure 1a) is always equal to zero. It could be proven analytically by Equation (8). The longitudinal component of SAM of the beam with V-line singularity (Equation (11), Figure 1b) is equal to zero at the focal plane; however, it is non-zero in the vicinity of the focal plane ( $z \neq 0$ , Figure 6). The longitudinal component of SAM of the beam (Equation (16), Figure 1c) is non-zero both at the focal plane and in the vicinity of the focal plane (Figure 9). This effect of the investigated beams can be used to obtain pure longitudinal magnetization distributions in optomagnetic memory systems [7,8].

The investigated beams (Figure 1) have local linear polarization in the initial plane; however, in tight focus, there are regions with elliptical polarization (Figures 6 and 9). This effect is a particular case of the Hall effect (or spin-orbit conversion) at a tight focus [30–33].

## 5. Conclusions

In this work, the tight focusing of vector beams with azimuthal polarization and beams with V-line of polarization singularity was simulated numerically using the Richards–Wolf formulas. It was demonstrated that in a tight focus for these beams, there is no longitudinal component of the electric field. The absence of the longitudinal component of the electric field leads to the fact that the spin angular momentum vector contains only the longitudinal component. Previously, a similar effect was demonstrated only for azimuthally polarized beams. The possibility of experimental generation of the studied beams using a spatial light modulator was demonstrated.

**Author Contributions:** Conceptualization, S.S.S.; methodology, S.S.S.; software, S.S.S., N.N.K. and V.D.Z.; validation, V.V.K. and S.S.S.; formal analysis, S.S.S. and V.V.K.; investigation, S.S.S., N.N.K. and S.D.P.; resources, S.S.S. and S.D.P.; data curation, V.D.Z. and S.D.P.; writing—original draft preparation, S.S.S., N.N.K. and V.D.Z.; writing—review and editing, V.V.K.; visualization, S.S.S. and S.D.P.; supervision, V.V.K.; project administration, V.V.K.; funding acquisition, V.V.K. All authors have read and agreed to the published version of the manuscript.

**Funding:** The work was supported by the Russian Science Foundation grant No. 23-12-00236 (in part of the experiment) and within the framework of the State assignment of the Federal Scientific Research Center “Crystallography and Photonics” of the Russian Academy of Sciences (in terms of theory).

**Institutional Review Board Statement:** Not applicable.

**Informed Consent Statement:** Not applicable.

**Data Availability Statement:** The data presented in this study are available on request from the corresponding author. The data are not publicly available due to privacy.

**Conflicts of Interest:** The authors declare no conflict of interest.

## References

1. Zhan, Q. Cylindrical vector beams: From mathematical concepts to applications. *Adv. Opt. Photonics* **2009**, *1*, 1–57. [[CrossRef](#)]
2. Hao, X.; Kuang, C.; Wang, T.; Liu, X. Phase encoding for sharper focus of the azimuthally polarized beam. *Opt. Lett.* **2010**, *35*, 3928–3930. [[CrossRef](#)]
3. Yuan, G.H.; Wei, S.B.; Yuan, X.C. Nondiffracting transversally polarized beam. *Opt. Lett.* **2011**, *36*, 3479. [[CrossRef](#)]
4. Kroychuk, M.K.; Shorokhov, A.S.; Yagudin, D.F.; Shilkin, D.A.; Smirnova, D.A.; Volkovskaya, I.; Shcherbakov, M.R.; Shvets, G.; Fedyanin, A.A. Enhanced Nonlinear Light Generation in Oligomers of Silicon Nanoparticles under Vector Beam Illumination. *Nano Lett.* **2020**, *20*, 3471–3477. [[CrossRef](#)]
5. Kroychuk, M.K.; Yagudin, D.F.; Shorokhov, A.S.; Smirnova, D.A.; Volkovskaya, I.I.; Shcherbakov, M.R.; Shvets, G.; Kivshar, Y.S.; Fedyanin, A.A. Tailored Nonlinear Anisotropy in Mie-Resonant Dielectric Oligomers. *Adv. Opt. Mater.* **2019**, *7*, 1900447. [[CrossRef](#)]

6. Sharif, V.; Pakarzadeh, H. High-performance surface plasmon resonance fiber sensor based on cylindrical vector modes. *Sci. Rep.* **2023**, *13*, 4563. [[CrossRef](#)]
7. Khorsand, A.R.; Savoini, M.; Kirilyuk, A.; Kimel, A.V.; Tsukamoto, A.; Itoh, A.; Rasing, T. Role of Magnetic Circular Dichroism in All-Optical Magnetic Recording. *Phys. Rev. Lett.* **2012**, *108*, 127205. [[CrossRef](#)]
8. Ignatyeva, D.O.; Davies, C.S.; Sylgacheva, D.A.; Tsukamoto, A.; Yoshikawa, H.; Kapralov, P.O.; Kirilyuk, A.; Belotelov, V.I.; Kimel, A.V. Plasmonic layer-selective all-optical switching of magnetization with nanometer resolution. *Nat. Commun.* **2019**, *10*, 4786. [[CrossRef](#)]
9. Nie, Z.; Ding, W.; Li, D.; Zhang, X.; Wang, Y.; Song, Y. Spherical and sub-wavelength longitudinal magnetization generated by  $4\pi$  tightly focusing radially polarized vortex beams. *Opt. Express* **2015**, *23*, 690. [[CrossRef](#)]
10. Udhayakumar, M.; Prabakaran, K.; Rajesh, K.B.; Jaroszewicz, Z.; Belafhal, A. Generating sub wavelength pure longitudinal magnetization probe and chain using complex phase plate. *Opt. Commun.* **2018**, *407*, 275–279. [[CrossRef](#)]
11. Wang, S.; Li, X.; Zhou, J.; Gu, M. Ultralong pure longitudinal magnetization needle induced by annular vortex binary optics. *Opt. Lett.* **2014**, *39*, 5022–5025. [[CrossRef](#)] [[PubMed](#)]
12. Nie, Z.; Ning, Z.; Liu, X.; Zhang, Y.; Wang, H.; Cao, E.; Yan, W. Creating multiple ultra-long longitudinal magnetization textures by strongly focusing azimuthally polarized circular Airy vortex beams. *Opt. Express* **2023**, *31*, 19089–19101. [[CrossRef](#)] [[PubMed](#)]
13. Gong, L.; Wang, L.; Zhu, Z.; Wang, X.; Zhao, H.; Gu, B. Generation and manipulation of super-resolution spherical magnetization chains. *Appl. Opt.* **2016**, *55*, 5783. [[CrossRef](#)]
14. Nie, Z.; Ding, W.; Shi, G.; Li, D.; Zhang, X.; Wang, Y.; Song, Y. Achievement and steering of light-induced sub-wavelength longitudinal magnetization chain. *Opt. Express* **2015**, *23*, 21296. [[CrossRef](#)]
15. Yan, W.; Nie, Z.; Zhang, X.; Wang, Y.; Song, Y. Magnetization shaping generated by tight focusing of azimuthally polarized vortex multi-Gaussian beam. *Appl. Opt.* **2017**, *56*, 1940–1946. [[CrossRef](#)]
16. Yan, W.; Nie, Z.; Liu, X.; Lan, G.; Zhang, X.; Wang, Y.; Song, Y. Dynamic control of transverse magnetization spot arrays. *Opt. Express* **2018**, *26*, 16824. [[CrossRef](#)] [[PubMed](#)]
17. Zand, M.; Miri, M.; Sadrara, M. Pure magnetic hotspots via hollow silicon nanoparticles illuminated by cylindrical vector beams. *J. Appl. Phys.* **2023**, *133*, 093101. [[CrossRef](#)]
18. Miao, Y.; Wang, L.; Zhang, Q.; Sun, X.; Gao, X.; Wan, J.; Zhuang, S. Tight-focusing properties of propagable fractional-order vector vortex beams. *J. Opt. Soc. Am. B* **2023**, *40*, 1113. [[CrossRef](#)]
19. Stafeev, S.S.; Nalimov, A.G.; Zaitsev, V.D.; Kotlyar, V.V. Tight focusing cylindrical vector beams with fractional order. *J. Opt. Soc. Am. B* **2021**, *38*, 1090. [[CrossRef](#)]
20. Ma, C.; Song, T.; Chen, R.; Li, H.; Li, X. Shaping focal field by grafted polarization. *Opt. Express* **2023**, *31*, 8120. [[CrossRef](#)]
21. Wang, J.; Dong, F.; Zhang, K.; Zhou, Y.; Song, Z.; Hu, H.; Xu, L.; Jiang, H.; Liang, G.; Zhang, Z.; et al. Generating a Superoscillation Three-Dimensional Hollow Spot by Polarization Manipulation. *Phys. Rev. Appl.* **2023**, *19*, 044069. [[CrossRef](#)]
22. Kotlyar, V.V.; Stafeev, S.S.; Nalimov, A.G.; O’Faolain, L. Subwavelength grating-based spiral metalens for tight focusing of laser light. *Appl. Phys. Lett.* **2019**, *114*, 141107. [[CrossRef](#)]
23. Richards, B.; Wolf, E. Electromagnetic Diffraction in Optical Systems. II. Structure of the Image Field in an Aplanatic System. *Proc. R. Soc. Lond. Ser. A* **1959**, *253*, 358–379. [[CrossRef](#)]
24. Pereira, S.F.; van de Nes, A.S. Superresolution by means of polarisation; phase and amplitude pupil masks. *Opt. Commun.* **2004**, *234*, 119–124. [[CrossRef](#)]
25. Davidson, N.; Bokor, N. High-numerical-aperture focusing of radially polarized doughnut beams with a parabolic mirror and a flat diffractive lens. *Opt. Lett.* **2004**, *29*, 1318–1320. [[CrossRef](#)]
26. Freund, I. Polarization singularity indices in Gaussian laser beams. *Opt. Commun.* **2002**, *201*, 251–270. [[CrossRef](#)]
27. Khonina, S.N.; Volotovskiy, S.G. Controlling the contribution of the electric field components to the focus of a high-aperture lens using binary phase structures. *J. Opt. Soc. Am. A* **2010**, *27*, 2188–2197. [[CrossRef](#)]
28. Khonina, S.N. Simple phase optical elements for narrowing of a focal spot in high-numerical-aperture conditions. *Opt. Eng.* **2013**, *52*, 091711. [[CrossRef](#)]
29. Stafeev, S.S.; Kotlyar, V.V.; Nalimov, A.G.; Kozlova, E.S. The Non-Vortex Inverse Propagation of Energy in a Tightly Focused High-Order Cylindrical Vector Beam. *IEEE Photonics J.* **2019**, *11*, 4500810. [[CrossRef](#)]
30. Kotlyar, V.; Stafeev, S.; Zaitsev, V.; Kozlova, E. Spin-Orbital Conversion with the Tight Focus of an Axial Superposition of a High-Order Cylindrical Vector Beam and a Beam with Linear Polarization. *Micromachines* **2022**, *13*, 1112. [[CrossRef](#)]
31. Nechayev, S.; Eismann, J.S.; Leuchs, G.; Banzer, P. Orbital-to-spin angular momentum conversion employing local helicity. *Phys. Rev. B* **2019**, *99*, 075155. [[CrossRef](#)]
32. Stafeev, S.S.; Nalimov, A.G.; Kovalev, A.A.; Zaitsev, V.D.; Kotlyar, V.V. Circular Polarization near the Tight Focus of Linearly Polarized Light. *Photonics* **2022**, *9*, 196. [[CrossRef](#)]
33. Shu, W.; Lin, C.; Wu, J.; Chen, S.; Ling, X.; Zhou, X.; Luo, H.; Wen, S. Three-dimensional spin Hall effect of light in tight focusing. *Phys. Rev. A* **2020**, *101*, 23819. [[CrossRef](#)]

**Disclaimer/Publisher’s Note:** The statements, opinions and data contained in all publications are solely those of the individual author(s) and contributor(s) and not of MDPI and/or the editor(s). MDPI and/or the editor(s) disclaim responsibility for any injury to people or property resulting from any ideas, methods, instructions or products referred to in the content.